Development of a green reversibly photoswitchable variant of Eos fluorescent protein with fixation resistance

Mitsuo Osuga, Tamako Nishimura, and Shiro Suetsugu*
Nara Institute of Science and Technology, Ikoma 630-0192, Japan

ABSTRACT **Superresolution microscopy determines the localization of fluorescent proteins with high precision, beyond the diffraction limit of light. Superresolution microscopic techniques include photoactivated localization microscopy (PALM), which can localize a single protein by the stochastic activation of its fluorescence. In the determination of single-molecule localization by PALM, the number of molecules that can be analyzed per image is limited. Thus, many images are required to reconstruct the localization of numerous molecules in the cell. However, most fluorescent proteins lose their fluorescence upon fixation. Here, we combined the amino acid substitutions of two Eos protein derivatives, Skylan-S and mEos4b, which are a green reversibly photoswitchable fluorescent protein (RSFP) and a fixation-resistant green-to-red photoconvertible fluorescent protein, respectively, resulting in the fixation-resistant Skylan-S (frSkylan-S), a green RSFP. The frSkylan-S protein is inactivated by excitation light and reactivated by irradiation with violet light, and retained more fluorescence after aldehyde fixation than Skylan-S. The qualities of the frSkylan-S fusion proteins were sufficiently high in PALM observations, as examined using α-tubulin and clathrin light chain. Furthermore, frSkylan-S can be combined with antibody staining for multicolor imaging. Therefore, frSkylan-S is a green fluorescent protein suitable for PALM imaging under aldehyde-fixation conditions.**

Monitoring Editor
Jennifer Lippincott-Schwartz
Howard Hughes Medical Institute

Received: Feb 3, 2021
Revised: Aug 23, 2021
Accepted: Sep 1, 2021

INTRODUCTION

Superresolution microscopy has achieved imaging with extremely high resolution using optical microscopes. The optical resolution is limited by the Abbe diffraction limit of the light, and thus the spatial resolution of an image, for example, by ~400 nm light, is restricted to ~150–200 nm. This optical limit of image resolution has been overcome with various superresolution microscopies, including structured illumination microscopy (SIM) (Gustafsson, 2000), stimulated emission depletion microscopy (STED) (Hell and Wichmann, 1994; Klar *et al.*, 2000), and single-molecule localization microscopy (SMLM) (Betzig *et al.*, 2006; Rust *et al.*, 2006). STED directly improved the optical resolution, while SIM and SMLM achieved spatial accuracy below the optical resolution by image reconstruction.

The widely used SMLM methods are stochastic optical reconstruction microscopy (STORM) (Rust *et al.*, 2006) and photoactivated localization microscopy (PALM) (Betzig *et al.*, 2006). STORM uses photoswitchable dyes that chemically label antibodies and nucleic acids (Heilemann *et al.*, 2005; Bates *et al.*, 2007; van de Linde *et al.*, 2011), whereas PALM was named after photoactivatable fluorescent proteins (PA-FPs), including Kaede, Dronpa, and EosFP (Habuchi *et al.*, 2005; Lippincott-Schwartz and Patterson, 2009; Bourgeois *et al.*, 2012; Shcherbakova *et al.*, 2014).

The SMLM image is reconstructed using the spatial coordinates of the observed molecules. The determination of the coordinates requires single-molecule observation, but the density of proteins is normally higher than that suitable for such observations; that is, the spacing is shorter than the diffraction limit of light. Thus, the

This article was published online ahead of print in MBoC in Press (http://www.molbiolcell.org/cgi/doi/10.1091/mbc.E21-01-0044).

Conflict of interest: The authors declare no competing financial interests.

Author contributions: M.O., T.N., and S.S. performed the biochemical and cell biological analyses. T.N. and S.S. supervised the project. M.O., T.N., and S.S. wrote the manuscript.

*Address correspondence to: Shiro Suetsugu (suetsugu@bs.naist.jp).

Abbreviations used: CLTA, clathrin light chain A; frSkylan, fixation-resistant Skylan; FWHM, full width at half-maximum; GA, glutaraldehyde; PA-FP, photoactivatable fluorescent protein; PALM, photoactivated localization microscopy; PFA, paraformaldehyde; RSFP, reversibly photoswitchable fluorescent protein.

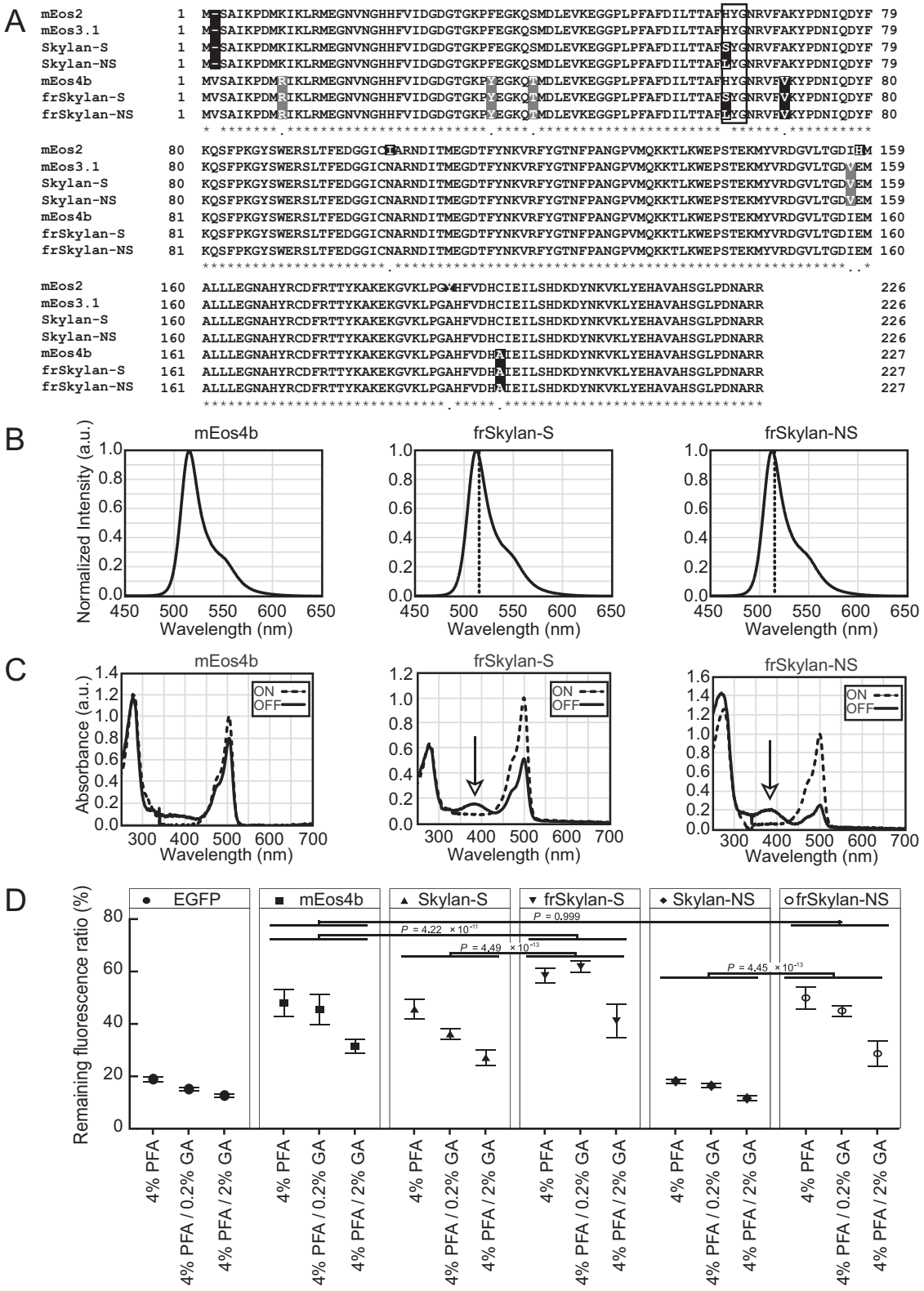

FIGURE 1: Properties of frSkylans. (A) Amino acid sequences of frSkylans and other EosFP-derived PA-FPs. The rectangle indicates the residues in the chromophore region. The differences in amino acid residues are highlighted. (B) Fluorescence emission spectra of mEos4b, frSkylan-S, and frSkylan-NS upon exposure to 430 nm excitation light, normalized at their emission maxima. Dashed lines show the emission maximum of mEos4b. (C) Absorption spectra of mEos4b, frSkylan-S, and frSkylan-NS in the ON and OFF states. Absorption spectra of the purified PA-FPs were measured in their ON state; that is, without any treatment. The OFF state was created by irradiation with 488 nm light for 10 min. Absorbances at ~500 nm in frSkylans, but not in mEos4b, decreased after irradiation with 488 nm light. The arrows indicate the increase in the absorbance at the OFF state. These absorption spectra were normalized at their

fluorophore labels of the molecules need to be inactivated and reactivated or activated from the nonobservable state. The blinking or activatable fluorophores by light irradiation enable the observations of sparsely populated fluorophores among all the labeled molecules (Betzig *et al.*, 2006; Rust *et al.*, 2006). The images are then reconstructed by the coordinates of the molecules, where each molecule localization has accuracy beyond the diffraction limit of light. The reconstruction requires a large number of coordinates; that is, many images. However, the collection of numerous images necessitates a longer acquisition time. Thus, the use of fixed cells is often preferred.

Fixation by commonly used aldehydes, including formaldehyde, paraformaldehyde (PFA), and glutaraldehyde (GA), causes the loss of fluorescent signals and photoactivatable ability (Joosen *et al.*, 2014; Johnson and Kaufmann, 2017). Therefore, the development of mEos4b, which is resistant to fixation, greatly improved the quality of reconstructed images in PALM (Paez-Segala *et al.*, 2015). The mEos4b protein is a derivative of EosFP, which is a tetrameric green-to-red photoconvertible fluorescent protein found in the stony coral *Lobophyllia hemprichii* (Wiedenmann *et al.*, 2004). A variant of EosFP, mEos2, is monomeric and shows better fluorescence at 37°C than monomeric EosFP (mEosFP) (McKinney *et al.*, 2009). mEos4b was subsequently developed from mEos2 by amino acid substitutions with less nucleophilicity, which reduced the surface reactivity and improved the thermodynamic stability, resulting in more robust resistance to fixation by aldehyde or OsO_4 and highlighting its utility for PALM imaging after chemical fixation (Paez-Segala *et al.*, 2015). mEos4b has a long-lived dark state and is suitable for SMLM (De Zitter *et al.*, 2019, 2020). However, photoconvertible fluorescent proteins occupy a wide range of wavelengths, and their applications in multicolor imaging are limited.

Reversibly photoswitchable fluorescent proteins (RSFPs) have a limited range of wavelengths. Green RSFPs include the stony coral *Pectiniidae* protein Dronpa (Ando *et al.*, 2004) and the Eos derivatives Skylan-S (Zhang *et al.*, 2015) and -NS (Zhang *et al.*, 2016), in which fluorescence states can be turned ON or OFF through *cis–trans* isomerization by light irradiation (Hutchison *et al.*, 2017). RSFPs can emit fluorescence multiple times with adequate inactivation and reactivation by excitation and activation lights, respectively, allowing the detection of several signals from a single fluorophore and leading to robust image reconstruction. Skylan-S and Skylan-NS have been applied for superresolution optical fluctuation imaging (SOFI) (Dertinger *et al.*, 2009; Zhang *et al.*, 2015) and nonlinear-SIM (Lu-Walther *et al.*, 2016; Zhang *et al.*, 2016), respectively. However, the contrast and fluorescence of most of the RSFPs, including Skylans, decreases upon chemical fixation (Shinoda *et al.*, 2019), thus limiting their applications.

In this study, we developed fixation-resistant green RSFPs, frSkylan-S and frSkylan-NS, by combining the amino acid substitutions of mEos4b and Skylans. We found that frSkylan-S and frSkylan-NS had greater aldehyde-fixation resistance in vitro than Skylan-S and Skylan-NS, respectively. Furthermore, we showed that frSkylan-S is brighter than frSkylan-NS and thus suitable for PALM imaging.

RESULTS AND DISCUSSION

The amino acid sequences of the green RSFPs

Skylans are green RSFPs (Zhang *et al.*, 2015, 2016) that were developed by amino acid substitutions in the chromophore of mEos3.1, a monomeric and brighter version of mEos2 (Zhang *et al.*, 2012). Accordingly, Skylan-S and Skylan-NS were mEos3.1-H62S and mEos3.1-H62L, respectively. On the other hand, mEos4b was developed by substitutions of amino acid residues primarily on the protein surface of mEos2 (Paez-Segala *et al.*, 2015). Therefore, we introduced amino acid substitutions into the chromophore of mEos4b in a manner analogous to the Skylans, resulting in mEos4b-H63S and mEos4b-H63L, which we named frSkylan-S and frSkylan-NS, respectively, because of their fixation resistance (described below). The amino acid sequences of these mEos derivatives are shown in Figure 1A.

Characterization of frSkylans

To characterize the photophysical properties of frSkylans, we performed spectroscopic measurements using the purified proteins in comparison with EGFP and mEos4b. The maximum emission wavelengths of frSkylan-S (512.9 nm) and frSkylan-NS (513.3 nm) were slightly shifted to a shorter wavelength than that of mEos4b (516.1 nm). The fluorescence spectra of these proteins were similar (Table 1; Figure 1B). Moreover, the maximum absorption wavelengths of frSkylan-S (499.5 nm) and frSkylan-NS (500.0 nm) also slightly shifted to a shorter wavelength than that of mEos4b (504.0 nm; Table 1). The quantum yield, molar extinction coefficient, and brightness of frSkylans were comparable to those of mEos4b, but frSkylan-S was brighter than frSkylan-NS (Table 1). The lifetimes of frSkylan-S (2.93 ns) and frSkylan-NS (2.88 ns) were shorter than that of mEos4b (3.26 ns), as measured by fluorescence lifetime imaging microscopy (Table 1). These results suggested that the H63S and H63L substitutions affected the fluorescence properties of these mEos4b proteins.

Reversible photoswitching by *cis–trans* and *trans–cis* photoisomerization is caused by light irradiation for excitation and activation, shifting from the ON state to the OFF state and the OFF state to the ON state, respectively (Pennacchietti *et al.*, 2018). X-ray crystallography revealed that the chromophore structure of Skylan-NS is altered by *cis–trans* photoisomerization via excitation light irradiation (Hutchison *et al.*, 2017). Thus, we examined whether frSkylans had photoswitching ability by monitoring their absorption spectra upon irradiation with 488 nm light (Figure 1C). As shown for Skylans (Zhang *et al.*, 2015, 2016), the absorbance at the absorption maxima of frSkylans was expected to be decreased by the excitation light (488 nm) and then increased by the activation light (405 nm). We found that the peak absorbance of frSkylans was dramatically reduced upon excitation by light irradiation (Figure 1C) in a manner similar to that of Skylans (Supplemental Figure S1). Importantly, the absorbance peak of frSkylans at approximately 380 nm appeared after the irradiation with 488 nm light (arrowheads in Figure 1C), indicating the photoswitching by the absorption of the UV light, as previously described for Skylans (Supplemental Figure S1). mEos4b did not exhibit a marked change in the absorbance upon the irradiation

absorption maximum. These spectra have an abnormal spike at around 340 nm because the light source was switched from the halogen lamp to the deuterium lamp at 340.8 nm while measuring the absorption. (D) Fluorescence of the PA-FPs in the fixation reagents. Fluorescent proteins were incubated in PBS, with or without PFA and GA, at 37°C for 30 min. The fluorescence spectra were then examined in the presence or absence of fixatives. The fluorescence intensity at the maximum emission wavelength in the presence of fixatives was compared with that in the absence of fixatives, shown by the means ± SD ($n = 4$). *P* values were determined by two-way ANOVA with Tukey's multiple comparisons tests.

Characteristic of protein:	EGFP	mEos4b (green)	Skylan-S	frSkylan-S	Skylan-NS	frSkylan-NS
Absorption, nm	488.5	504.0	499.0	499.5	499.5	500.0
Emi, nm	510.5	516.1	513.1	512.9	512.7	513.3
QY	(0.60)	0.77	0.76	0.80	0.67	0.68
ε-max, $M^{-1}cm^{-1}$	62,700	97,000	94,200	95,400	86,900	99,100
Brightness	37.6	74.7	72.0	76.3	57.8	67.4
Mature fraction, %	70	66	75	73	77	77
Lifetime, ns	2.55 ± 0.015	3.26 ± 0.015	2.871 ± 0.009	2.93 ± 0.010	2.93 ± 0.019	2.88 ± 0.010
Photofatigue half decay without fixation, cycle	N/A	N/A	7	5	16	11
Photofatigue half decay with fixation, cycle	N/A	N/A	3	2	1	2

The maximum absorption wavelength, maximum emission wavelength (Emi), quantum yield (QY), and molar extinction coefficient at the maximum absorption wavelength (ε-max) were measured in PBS (pH 7.4) for the ON states for the RSFPs or in the green fluorescence-emitting state for mEos4b. QYs were determined relative to the reported value of EGFP (0.60) (Sarkisyan *et al.*, 2015). Brightness was calculated as ε-max × *QY* × 10^{-3}. The mature fraction was defined as the percentage of the mature chromophore of the purified protein. Lifetimes were measured in HeLa cells expressing fluorescent protein–tagged CLTA, and the values were weight averaged. The photofatigue half decay is the switching cycle at which MAX intensity reaches half its maximum with or without fixation.

TABLE 1: Photo-characteristics of fluorescent proteins.

(Figure 1C). These results suggested that frSkylans shared photoswitching ability similar to that of Skylans.

Fixation resistance of frSkylans

The fluorescence of the frSkylan proteins in the presence of aldehyde fixative was examined in comparison with that in the absence of fixative. As previously reported (Paez-Segala *et al.*, 2015), the mEos4b protein was resistant to fixation, and its fluorescence in the presence of aldehydes was robustly maintained as compared with that of EGFP (Figure 1D). The frSkylan-S and -NS proteins were more resistant to fixation than the Skylan-S and -NS proteins, respectively (Figure 1D), suggesting that the surface amino acid residues of the mEos4b protein contributed to the fixation resistance.

The fluorescence of frSkylan-S that persisted after fixation, in comparison with that without fixation, was the largest among the proteins examined, suggesting its stronger resistance to fixation (Figure 1D). The remaining fluorescence of frSkylan-S was higher with 4% PFA than with 4% PFA + 2% GA but was similar to that with 4% PFA + 0.2% GA (Figure 1D). The resistance of frSkylan-NS was comparable to that of mEos4b. frSkylan-S, frSkylan-NS, and mEos4b contain serine, leucine, and histidine at residue 63, respectively (Figure 1A), which may be responsible for the differences in the chromophore stabilization upon aldehyde fixation.

We next examined the photoswitching kinetics of RSFPs embedded within polyacrylamide gels. The gels were treated with phosphate-buffered saline (PBS) containing 4% PFA or with PBS alone and then washed to remove the fixative (Figure 2A). After the measurement of the photoswitching, the fitting of the exponential decay equation ($y = a \times \exp(-bx) + c$) to each cycle was performed to obtain the photoswitching parameters. The photofatigue resistances of Skylan-S and frSkylan-S upon the aldehyde fixation were higher than those of Skylan-NS and frSkylan-NS, as shown by the max intensity of fluorescence over cycles (Figure 2B; Table 1). The exponential decay constant (*b*) of the RSFPs in PBS increased as the photoswitching cycles increased (Figure 2C). Interestingly, the exponential decay constant of frSkylan-S was the smallest among the RSFPs (Figure 2C). With the treatment of 4% PFA, the exponential decay constants of frSkylan-S and frSkylan-NS were relatively unchanged (Figure 2C), whereas that of Skylan-S slightly increased and that of SkylanNS decreased (Figure 2C). In PBS, the photoswitching ON/OFF contrasts ($(a + c) / c$) of the RSFPs were decreased as the photoswitching cycles increased (Figure 2D). By 4% PFA, the ON/OFF contrast over the cycles for frSkylan-S increased, but that of frSkylan-NS decreased (Figure 2D). The ON/OFF contrast of the parental Skylans decreased as the cycles increased, suggesting the improvement of fixation resistance, especially for frSkylan-S (Figure 2D). Accordingly, the OFF-state background; that is, the baseline intensity ratio ($c / (a + c)$), of the fixed frSkylan-S decreased with increasing photoswitching cycles (Figure 2E).

Superresolution imaging of the frSkylan-S fusion proteins

To assess whether frSkylan-S is applicable to superresolution microscopy, α-tubulin fused to frSkylan-S (frSkylan-S-α-tubulin) was subjected to PALM imaging. The cells that stably expressed frSkylan-S-α-tubulin were fixed with 4% PFA + 0.2% GA, followed by PALM imaging. frSkylan-S-α-tubulin achieved sufficiently sparse blinking to allow the determination of the localization of each fluorescent signal, and the reconstruction of the coordinates of frSkylan-S-α-tubulin resulted in the images of tubulin (Figure 3, A and B). The full width at half-maximum (FWHM) of the tubulin filaments was measured by fitting a Gaussian function to the axis perpendicular to the filament line (Figure 3, C and D). The average FWHM of the frSkylan-S-α-tubulin

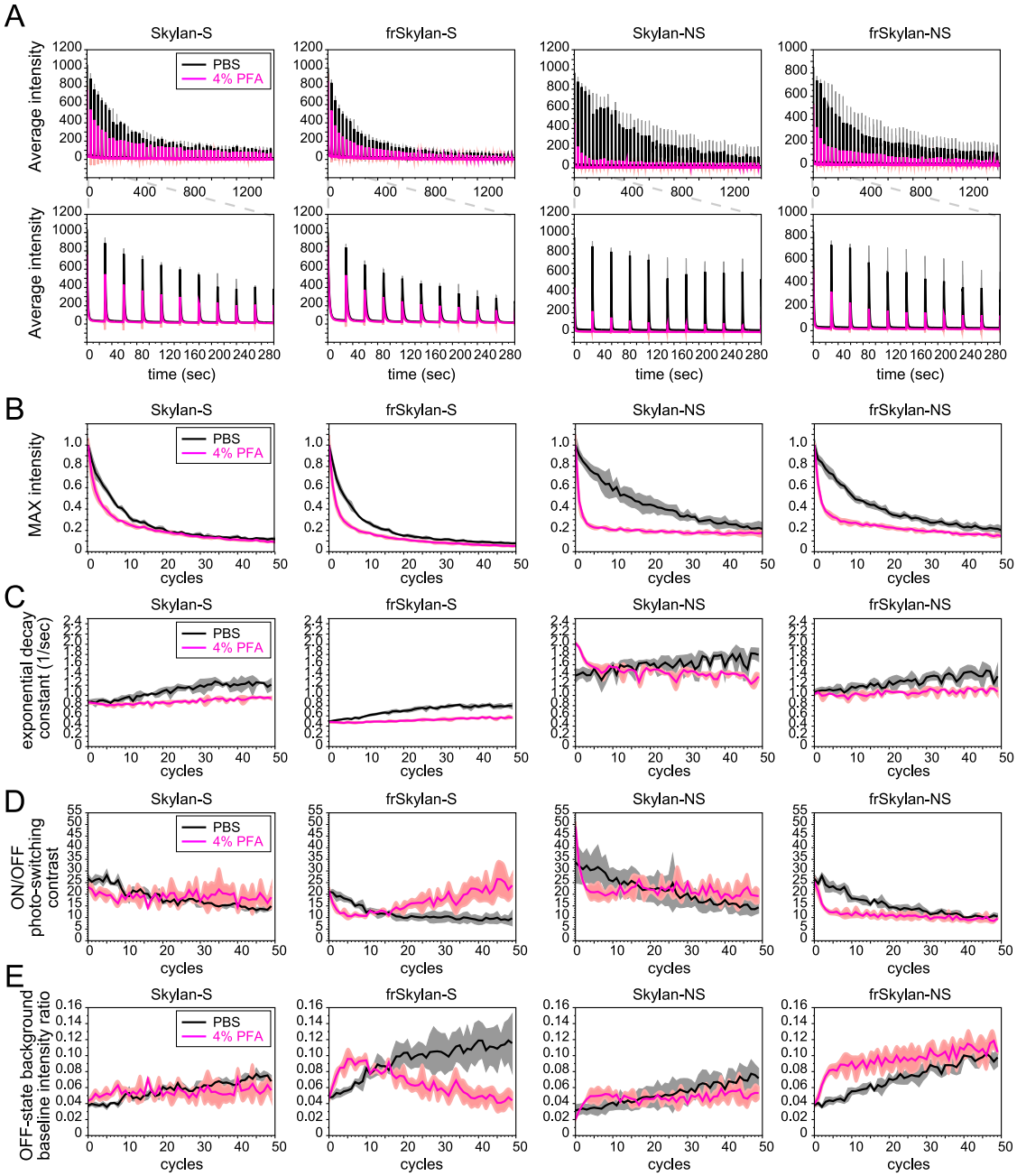

FIGURE 2: Photoswitching kinetics of frSkylans and Skylans with or without fixatives. (A) Averaged photoswitching kinetics of the RSFP proteins embedded in the acrylamide gels. Gels were incubated in PBS or PBS with 4% PFA for 10 min at room temperature, washed, and observed under a confocal microscope. Fluorescence images were continuously acquired by a 488 nm laser. Irradiation by a 405 nm laser was performed at 30 s intervals to activate fluorescence. Fluorescence intensity profiles for the initial 300 s are enlarged and shown at the bottom. Error bar: SD ($n = 3$). (B) Photoswitching fatigue of the RSFPs. The photoswitching curve from each cycle was fitted to the "exponential with offset" formula ($y = a \times \exp(-bx) + c$) to calculate the MAX intensity ($a + c$) of each cycle, and the decrease rate reflects the photoswitching fatigue resistance of RSFPs. These averaged MAX intensities were normalized by the initial values of cycles under each condition. Error bar: SD ($n = 3$). (C) Exponential decay constant of fluorescence in the photoswitching cycles of RSFPs. The averaged exponential decay constant (b) of each cycle is plotted with SD ($n = 3$). (D) Photoswitching ON/OFF contrast of RSFPs. The mean of the photoswitching ON/OFF contrast ($(a + c)/c$) was plotted with SD ($n = 3$). (E) OFF-state background of RSFPs. The mean of the baseline intensity ratio (OFF-state background) ($c / (a + c)$) was plotted with SD ($n = 3$).

microtubules was 66.0 ± 8.1 nm (Figure 3D; Supplemental Figure S2), which was superior to the result reported for mEos3.2-α-tubulin (median 109 nm) (Khan *et al.*, 2017). Therefore, frSkylan-S achieved adequate superresolved image acquisition of microtubules.

Clathrin light chain A (CLTA) was fused with frSkylan-S and tested for PALM imaging. In the reconstructed image of the clathrin light chain by SMLM, clathrin-coated pits and plaque-like structures were observed, as reported (Leyton-Puig *et al.*, 2017). The z-projected

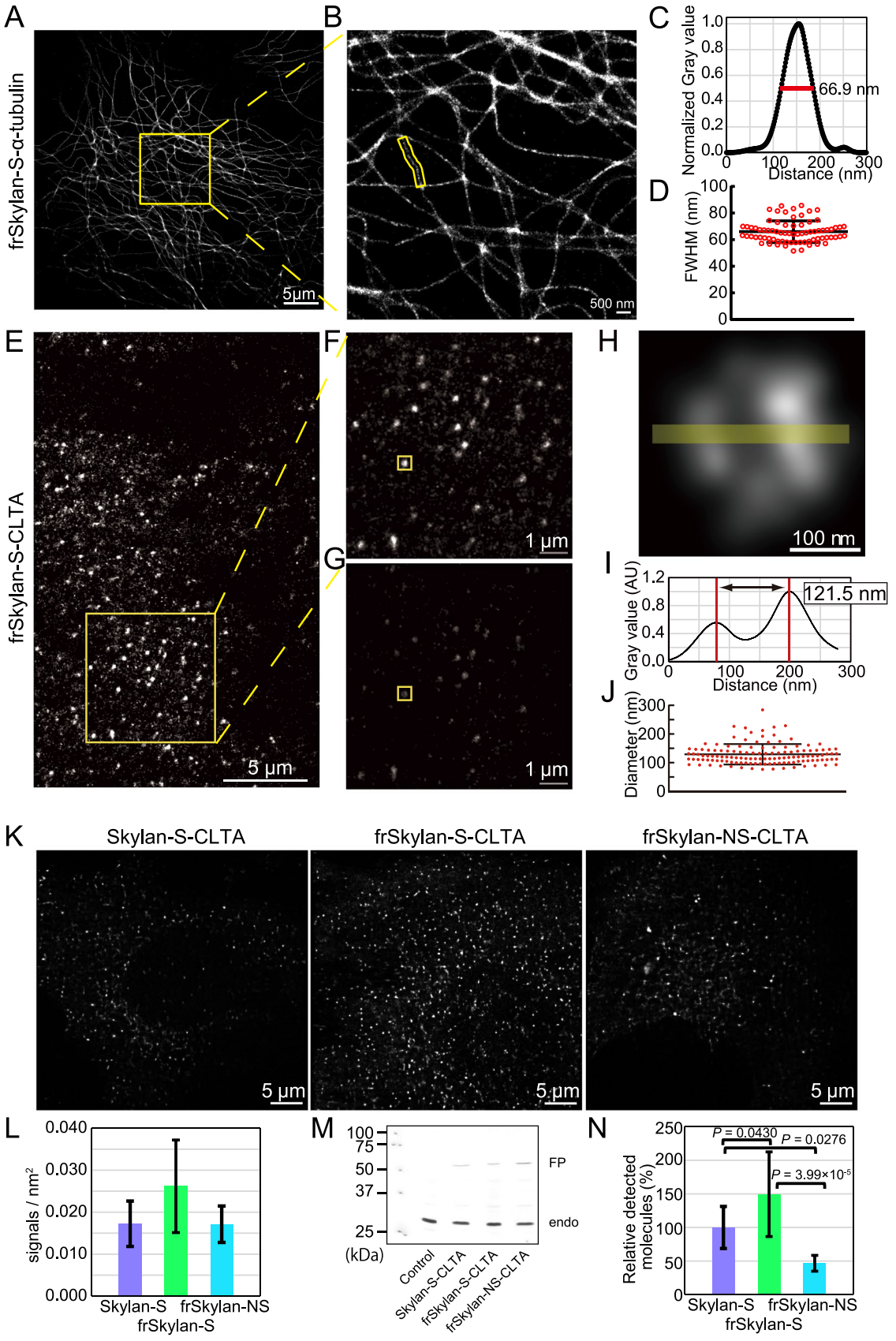

FIGURE 3: PALM imaging of frSkylan-S tagged with α-tubulin and CLTA. (A) Reconstructed image of frSkylan-S-α-tubulin by PALM imaging. frSkylan-S-α-tubulin stably expressed in HeLa cells was observed. Scale bar, 5 μm. (B) Enlarged image of A. The microtubule filament marked with yellow is a representative for the quantification of FWHM shown in C. Scale bar, 500 nm. (C) Signal density profile graph of the microtubule filament in B perpendicular to

reconstructed image of frSkylan-S-CLTA is shown in Figure 3E, and the highlighted area is magnified in Figure 3F. The 50-nm-thick section in Figure 3F is shown in Figure 3G, in which the highlighted area shows that frSkylan-S-CLTA was able to image the ring-like structure of a clathrin-coated pit (Figure 3H). The signal density profile indicated that the diameter of the ring-like structure was 121.5 nm (Figure 3I), consistent with that of the clathrin-coated pit determined by SMLM (Ehrlich *et al.*, 2004; Leyton-Puig *et al.*, 2017) (Figure 3J). These results indicated that frSkylan-S is suitable for PALM imaging under aldehyde fixation.

Then, we compared the efficiency of frSkylan-S with those of frSkylan-NS and Skylan-S in PALM imaging (Figure 3K). After the image reconstruction, the signal density of RSFP-fused clathrin was quantified (Figure 3L). The signal density was then normalized by the expression levels of RSFP-clathrin relative to endogenous CLTA (Figure 3, M and N). The frSkylan-S-CLTA produced the most signals; that is, the highest image quality compared with those tagged with frSkylan-NS or Skylan-S (Figure 3N).

To further confirm the advantages of using fixation, we tried to stain the cells expressing the frSkylan-S-CLTA with the antibody for α-tubulin, which was detected by the fluorescently labeled secondary antibody conjugated with Alexa dye. After superresolution imaging of frSkylan-S-CLTA and Alexa-labeled tubulin, the CLTA and α-tubulin localization signals were both clearly identified with the appropriate CLTA cluster diameters and the tubulin FWHMs (Figure 4, A and B), corroborating the usefulness of frSkylan-S in PALM imaging.

In this study, frSkylan-S showed the highest fixation resistance in vitro and provided a genetic label for the detection of proteins in PALM imaging. The numerous photon emissions per signal enable higher accuracy in SMLM (Betzig *et al.*, 2006). Thus, the slower photoswitching speed of frSkylan-S, as compared with those of Skylan-S and frSkylan-NS, was assumed to contribute to the imaging quality in PALM (Figures 2C and 3N). Furthermore, the higher switching fatigue resistance after the fixation and the better switching contrast of frSkylan-S in the increasing switching cycles appeared to be the possible reasons for the enhanced image quality of frSkylan-S in PALM (Figure 3, B and D). We confirmed that frSkylan-S could be utilized for the PALM imaging of microtubules and clathrin (Figure 3). In addition, the fixation resistance allowed the immunostaining of another protein, enabling the detection of two kinds of proteins (Figure 4). However, because the RSFPs in colors other than green are limited, the development of fluorescent proteins with different colors and fixation resistance will be required for multiprotein superresolution imaging by using RSFPs.

MATERIALS AND METHODS

Plasmid construction

The mEos4b cDNA was inserted into the pRSET-B vector (Paez-Segala *et al.*, 2015). pRSET-B-frSkylan-S and -frSkylan-NS were constructed by introducing point mutations in pRSET-B-mEos4b, using PrimeSTAR Max DNA polymerase (TaKaRa). To express frSkylan-S–tagged α-tubulin in mammalian cells, the EGFP gene in the pEGFP-Tub vector (Clontech) was replaced with mEos4b, and point mutations were introduced using PrimeSTAR Max DNA polymerase to construct pfrSkylan-S-Tub. To construct the frSkylan-S–tagged CLTA expression plasmid, named pEF1-frSkylan-S-CLTA, we first constructed a pEF1-mEos4b-CLTA vector by replacing EGFP of an EGFP-tagged CLTA-containing vector harboring the EF1-α promoter with mEos4b. We then introduced point mutations into the mEos4b sequences of pEF1-mEos4b-CLTA to construct pEF1-frSkylan-S-CLTA, pEF1-frSkylan-NS-CLTA, and pEF1-Skylan-S-CLTA. All plasmid ligations were performed using Gibson Assembly Master Mix (New England Biolabs).

Protein expression and purification

Escherichia coli BL21(DE3) cells were transformed with the above pRSET-B plasmids and cultured in 1 l of Studier autoinduction medium (Grabski *et al.*, 2005; Studier, 2005), with 50 μg/ml ampicillin at 37°C for 12–16 h, for the expression of fluorescent proteins. *E. coli* cell pellets were resuspended in 37.5 ml of native lysis buffer (50 mM NaH_2PO_4, 300 mM NaCl, 10 mM imidazole, pH 8.0) and sonicated using an ultrasonic homogenizer (Qsonica; Q700). After ultracentrifugation in an OPTIMA L-90K (Beckman Coulter; 45 Ti rotor) at 35,000 rpm (142,000 × *g*) for 35 min, the supernatants were mixed with a 1-ml bed volume of Ni-Sepharose 6 Fast Flow resin (GE Healthcare) on a rotary shaker for 30 min at 4°C. The resin was equilibrated with native lysis buffer and rotated. The resin was then placed in an open column (Bio-Rad; Econo-Pac column) and washed three times with 10 ml of the native wash buffer. The proteins were eluted twice with 500 μl of elution buffer (50 mM NaH_2PO_4, 300 mM NaCl, pH 8.0) supplemented with increasing concentrations of imidazole (50, 150, 250, 350, and 450 mM). The fractions containing the proteins of interest were dialyzed three times against PBS (pH 7.4) for 12 h at 4°C.

Measurement of the photo-characteristics of PA-FPs

The purified protein concentration was determined by using a bicinchoninic acid assay kit (Nacalai Tesque), and the protein ratio was calculated from the SDS–PAGE results. Absorption spectra from 250 to 700 nm were measured using a UV-1800 spectrometer

the microtubule with the FWHM is shown in red. (D) Distribution of the FWHM values of the microtubules in the reconstructed images. The FWHM values of 75 filaments were plotted. The bar indicates the mean ± SD. Filaments used for the quantification are shown in Supplemental Figure S2. (E–G) Reconstructed PALM image of frSkylan-S-CLTA stably expressed in cells. (E) Z-projected whole-cell image, (F) enlarged image of the area marked with the square in E, and (G) the 50-nm-thickness slice of F. (H) CLTA localization at the possible clathrin-coated pit in the 50 nm slice. The enlarged image of the area marked with the square in G is shown with the line for the profiling in I. (I) Intensity profile of the ring-like structure of the CLTA cluster in H. (J) Distribution of the diameters of the CLTA clusters. SR-Tesseler software was used for the cluster analysis, as described in *Materials and Methods*. The bar indicates the mean ± SD ($n = 129$). (K) Reconstructed PALM images of RSFP-tagged CLTAs that were stably expressed in cells. The cells were fixed by 4% PFA/2% GA/HEPES buffer for 20 min before PALM observation. Scale bars, 5 μm. (L) Average densities of the detected signals of CLTA tagged with the RSFPs in the CLTA cluster. Bars indicate the average ± SD ($n = 10$ cells). (M) Western blotting of the cells expressing CLTA tagged with the RSFPs, using an anti-CLTA antibody. Endo: endogenous CLTA; FP: RSFP-labeled CLTA. (N) Comparison of the relative numbers of detected molecules in the CLTA cluster, as normalized to the expression level of RSFP-CLTA. Bars indicate the weighted average ± SD ($n = 10$ cells). *P* values were determined by one-way ANOVA with Tukey's multiple comparisons tests.

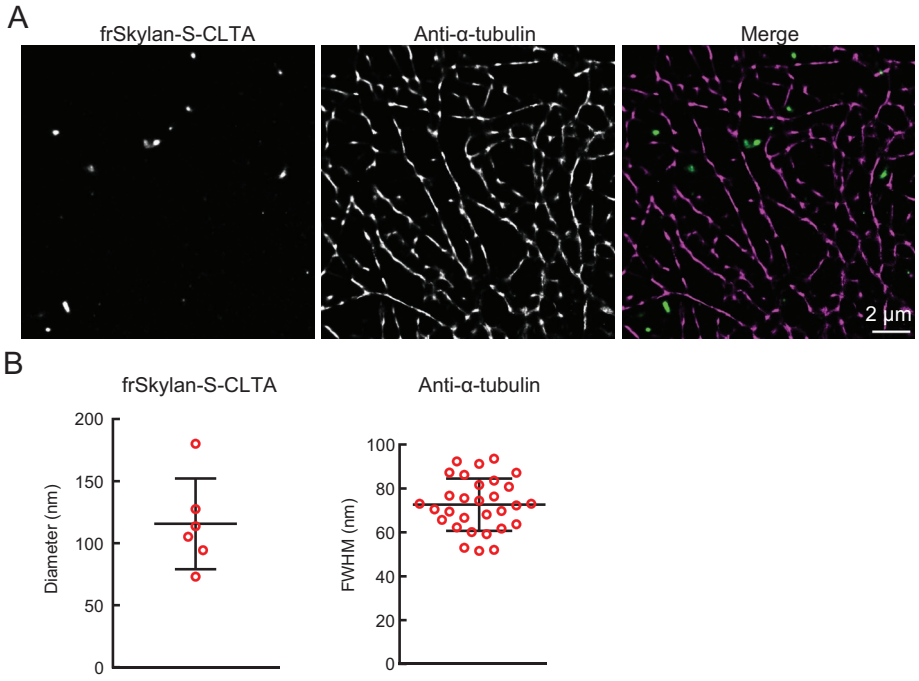

FIGURE 4: Multicolor superresolution observation for frSkylan-S-CLTA with immunostained α-tubulin. (A) Multicolor superresolution image of frSkylan-S-CLTA with immunostained α-tubulin. Cells stably expressing frSkylan-S-CLTA were fixed with 4% PFA/2% GA for 20 min, immunostained by an anti–α-tubulin antibody, and visualized by an Alexa 647–labeled anti-mouse $(Fab)_2$ antibody. Scale bar, 2 μm. (B) Quantification of the diameters of the CLTA clusters ($n = 6$) and the FWHM values of the microtubules by α-tubulin staining ($n = 30$), visualized by the multicolor superresolution observation shown in panel A. Bars indicate the mean ± SD.

(Shimadzu). Emission spectra were measured by excitation at 430 nm, using an FP-6500 fluorometer (JASCO).

The chromophore concentrations were measured using the alkali-denaturation method (Shaner *et al.*, 2013; Shinoda *et al.*, 2019). In brief, a double-concentration sample was prepared and mixed with equal amounts of 2 M NaOH. The absorbance of the mixed sample was then measured immediately, using a UV-1800 spectrometer. The molar extinction coefficient of the acquired peak absorbance at ~447 nm was assumed to be equivalent to that of the denatured original *Aequorea victoria* GFP (avGFP) chromophore (44,000 M^{-1} cm^{-1}) (Shinoda *et al.*, 2018), and thus the concentration of the chromophore was calculated.

The mature fraction was calculated as the concentration of chromophore divided by the concentration of total fluorescent protein, as previously described (Shinoda *et al.*, 2018). The molar extinction coefficient was calculated using the Beer–Lambert law (Absorbance = εcl), where ε is the molar extinction coefficient, c is the molar concentration, and l is the optical path length.

Fluorescence quantum yields were determined relative to the values reported for EGFP (0.60) (Sarkisyan *et al.*, 2015). Fluorescence spectra were acquired using 480 nm light, and the absorbance at 480 nm was measured for quantum yield calculations.

The photoswitching ability was evaluated by measuring the absorption spectra of the purified protein solution (ON state). The OFF state was induced by irradiation with 488 nm light for 10 min in the fluorometer, followed by another measurement of the absorption spectra (OFF state).

To evaluate the fixation resistance of the fluorescent protein, each purified protein was diluted to 1 μM in PBS (pH 7.4) with or without fixatives and incubated at 37°C for 30 min. The fluorescence was then measured using a fluorometer. Fixation resistance was calculated as the percentage of the maximum fluorescence intensity with fixatives relative to that without fixatives, as follows: 4% PFA in PBS, 4% PFA + 0.2% GA in PBS, and 4% PFA + 2% GA in PBS.

The lifetime of the fluorescent protein was measured using an SP8 FALCON confocal microscope (Leica). HeLa cells transfected with fluorescent protein–tagged CLTA were used, and the lifetimes of the CLTA fusion proteins were determined by fitting to the *n*-exponential reconvolution model with two exponential components. The weighted averages of the obtained lifetimes with χ^2 fittings under two were calculated. The sample sizes were five for EGFP, three for mEos4b, eight for Skylan-S, five for frSkylan-S, three for Skylan-NS, and four for frSkylan-NS.

Measurement of the photoswitching kinetics

Purified fluorescent proteins (final concentration: 39.7 μM) were mixed with 20.3% (wt/vol) acrylamide/bis mixed solution (37.5:1) containing 0.1% ammonium persulfate (APS) and 0.134% Tetramethylethylenediamine (TEMED), and then the mixture was solidified between 12 mm coverslips and parafilm for 40 min. The fluorescent protein–containing gel was removed from the coverslip and treated with PBS, with or without 4% PFA, for 10 min. After two washes with PBS for 3 min each, the gel was mounted onto a glass slide enclosed by adhesive tape and covered with a coverslip.

The photoswitching kinetics were analyzed using a confocal microscope (FV1000; Olympus) equipped with a 60× oil (NA 1.35) objective lens, 38.1 μW 488 nm laser, and 14.6 μW 405 nm laser. Fluorescent proteins were activated by a 405 nm laser at 30 s intervals and then monitored continuously using a 488 nm laser at room temperature (25°C). The area monitored by the 488 nm laser was 696.96 μm^2, and the area activated by the 405 nm laser was 136.78 μm^2. The average fluorescence intensity of the activated area was measured. The results from three independent positions were recorded for each fluorescent protein. The off-switching curve of each photoswitching cycle was fitted to the "exponential with offset" formula ($y = a \times \exp(-bx) + c$), using the solver plug-in of Excel (Microsoft) and the least-squares method, in which b is the exponential decay constant, $a + c$ is the max intensity, $(a + c)/c$ is the switching on/off contrast, and $c/(a + c)$ is the baseline intensity ratio.

Cell culture and transfection

HeLa cells (a generous gift from Tadaomi Takenawa, University of Tokyo) were grown in DMEM (Nacalai) supplemented with 10% fetal bovine serum (Hyclone), 63 μg/ml benzylpenicillin potassium, and 100 μg/ml streptomycin. HeLa cells were transfected with the above plasmids, using Lipofectamine 3000 (Thermo Fisher) according to the manufacturer's instructions, and selected using G418 (Roche Diagnostics) to obtain stably expressing single cell clones.

Western blotting

Western blotting was performed using an anti-clathrin light chain antibody (Proteintech; 10852-1-AP; 1:1000) and alkaline-phosphatase (AP)-conjugated anti-rabbit immunoglobulin G (IgG) (Promega), as well as AP substrate, consisting of 5-bromo-3-chloro-indolyl phosphate (Roche Diagnostics) and 4-nitro blue tetrazolium chloride (Roche Diagnostics) for detection. The signals were quantified using ImageJ software (National Institutes of Health [NIH]).

Immunostaining

HeLa cells stably expressing frSkylan-S–tagged CLTA were fixed with 4% PFA and 2% GA in buffer containing 30 mM HEPES (pH 7.4), 100 mM NaCl, and 2 mM $CaCl_2$, for 20 min at room temperature. After three washes with PBS, the cells were treated with 0.1% $NaBH_4$ in PBS for 7 min on ice. After three 5 min washes with PBS, the cells were blocked by blocking buffer containing 3% bovine serum albumin (BSA) and 0.2% Triton X-100 in PBS for 2 h at room temperature. The mouse anti–α-tubulin antibody (clone DM1A; CST; #3873; 1:1000) in blocking buffer was added to the cells and incubated for 1 h at room temperature. After five washes with wash buffer containing 0.2% BSA and 0.05% Triton X-100 in PBS, Alexa 647–labeled F(ab')$_2$-goat anti-mouse IgG (H+L) antibody (Invitrogen; A21237; 1:6400) was added and incubated for 1 h at room temperature. After five washes with the wash buffer and one wash with PBS, the cells were stored at 4°C in 1% (wt/vol) polyvinyl alcohol and 10 mM cysteamine in PBS until the PALM observation.

PALM imaging and analysis

HeLa cells stably expressing frSkylan-S-α-tubulin or CLTA were cultured in glass-based dishes. In the case of α-tubulin, the cells were simultaneously permeabilized with fixation by 30 mM HEPES buffer (pH 7.4) containing 4% PFA, 0.2% GA, 2 mM $CaCl_2$, 100 mM NaCl, and 0.5% Triton X-100 for 20 min at room temperature. HeLa cells stably expressing frSkylan-S-CLTA were fixed by the same solution without Triton X-100. Subsequently, the fixatives were quenched with 0.1% $NaBH_4$ in PBS for 7 min on ice, and then the cells were washed with PBS and soaked in PBS containing 1% (wt/vol) polyvinyl alcohol and 10 mM cysteamine. An N-STORM (Nikon) superresolution microscope equipped with a 100×/1.49 objective lens (Apo TIRF 100× Oil DIC N2; Nikon) and an EMCCD camera (iXon Du-897; ANDOR) was used to obtain 100,000 images of 256 × 256 pixels (40.96 × 40.96 μm), with a 16 ms exposure time. A 405 nm laser (CUBE 405-100C; Coherent) and a 488 nm laser (IMA101065ALS; Melles Griot) were used to activate frSkylan-S and detect its fluorescence, respectively. The acquired images were analyzed using NIS-Elements software (Nikon). These coordinate data were processed with ChriSTORM (Leterrier *et al.*, 2015) for reconstruction using ThunderSTORM (Ovesný *et al.*, 2014) with filtering, duplicate removal, drift correction by cross-correlation, and visualization by the normalized Gaussian method.

frSkylan-S-CLTA–expressing HeLa cells that were stained with α-tubulin were observed according to the reported procedure, with slight modifications (Olivier *et al.*, 2013; Tachikawa *et al.*, 2017). Briefly, the cells were soaked in PBS, supplemented with 10 mM Tris HCl, pH 7.5, 10% glucose, 10 mM cysteamine, 50 mM 2-mercaptoethanol, 2.5 mM protocatechuic acid, 2 mM cyclooctatetraene, and 50 mM protocatechuic dioxygenase just before the observation. A total of 40,000 fluorescence images were sequentially acquired, in which the first 20,000 images were of frSkylan-S-CLTA and the remaining 20,000 images were of α-tubulin. The 405 nm laser was used for the fluorophore activation, and the 488 and 647 nm lasers were used for the detection of frSkylan-S-CLTA and α-tubulin, respectively.

Quantification of the filament width of microtubules

The FWHM of the microtubules was determined as described previously (Virant *et al.*, 2018). Five regions of 10 × 10 μm squares were selected in a reconstructed image. In each region, 15 microtubules were randomly selected along the peak of the gray value, using the segmented line tool in ImageJ (NIH). Subsequently, each line width was set at 300 nm to cover the filament, and then the line was straightened using the straighten tool. Averaged intensity profiles perpendicular to the straightened line were obtained by a straight line that was 300 nm in width and 1 μm in length. To obtain the FWHM, the intensity profile was fitted to a Gaussian curve, and the obtained sigma value was multiplied by 2.35 (Virant *et al.*, 2018). In the multicolor PALM imaging, the 30 positions of microtubules shown in Figure 4A were measured by the same method as above.

Quantification of the CLTA cluster

Quantification was performed using SR-Tesseler software (Levet *et al.*, 2015; Staszowska *et al.*, 2018). In brief, a Voronoi diagram was generated by drawing bisector lines between each molecule, from which the molecular density was calculated. Next, the region where the molecular density was more than twofold, as compared with the average density in the entire region, was selected. A clathrin cluster was then defined as the area where the molecular density was more than twofold, as compared with the average density of the selected region. Among the CLTA clusters, those with areas of 7850–115,600 nm^2 were selected, because the typical cluster radius of clathrin-coated pits was 50–170 nm (Staszowska *et al.*, 2018), and then quantified for the diameter as described previously (Levet *et al.*, 2015).

To obtain the signal density, the clathrin signals/nm^2 in the clusters were calculated by the number of signals divided by the area in each determined cluster. The values of signals/nm^2 of clusters in the cell were averaged, giving the signal density of the cell. The averaged signals/nm^2 from 10 cells are shown in Figure 3L. The relative performances of the RSFPs were obtained by normalization to the amount of RSFP-CLTA, as determined by the endogenous CLTA amount, where the expression level of Skylan-S-CLTA was set to 100%. In the multicolor PALM imaging, the CLTA clusters in Figure 4A were measured by the same method as above.

Statistical analysis

Histograms and line charts are expressed as the mean ± SD, as indicated in the figure legends. Statistical analyses were performed using GraphPad Prism 7.02 software (GraphPad.com). The statistical significance for fixation resistance was examined by two-way analysis of variance (ANOVA) with Tukey's multiple comparisons tests, and that of the signal density of a CLTA cluster was examined by one-way ANOVA with Tukey's multiple comparisons tests. *P* values were adjusted for multiple tests using Tukey's method. The statistical significance was set at $P < 0.05$.

ACKNOWLEDGMENTS

This work was supported by the Japan Society for the Promotion of Science (JSPS) (KAKENHI, JP17H03674, JP17H06006) and Japan Science and Technology Agency (JST) Core Research for Evolutional Science and Technology (CREST) (JPMJCR1863). We thank K. Oono-Yakura for technical support and other laboratory members for discussions.

REFERENCES

Ando R, Mizuno H, Miyawaki A (2004). Regulated fast nucleocytoplasmic shuttling was observed by reversible protein highlighting. Science 306, 1370–1373.

Bates M, Huang B, Dempsey GT, Zhuang X (2007). Multicolor super-resolution imaging with photo-switchable fluorescent probes. Science 317, 1749–1753.
Betzig E, Patterson GH, Sougrat R, Lindwasser OW, Olenych S, Bonifacino JS, Davidson MW, Lippincott-Schwartz J, Hess HF (2006). Imaging intracellular fluorescent proteins at nanometer resolution. Science 313, 1642–1645.
Bourgeois D, Regis-Faro A, Adam V (2012). Photoactivated structural dynamics of fluorescent proteins. Biochem Soc Trans 40, 531–538.
Dertinger T, Colyer R, Iyer G, Weiss S, Enderlein J (2009). Fast, background-free, 3D super-resolution optical fluctuation imaging (SOFI). Proc Natl Acad Sci USA 106, 22287–22292.
De Zitter E, Ridard J, Thédié D, Adam V, Lévy B, Byrdin M, Gotthard G, Van Meervelt L, Dedecker P, Demachy I, Bourgeois D (2020). Mechanistic investigations of green mEos4b reveal a dynamic long-lived dark state. J Am Chem Soc 142, 10978–10988.
De Zitter E, Thédié D, Mönkemöller V, Hugelier S, Beaudouin J, Adam V, Byrdin M, Van Meervelt L, Dedecker P, Bourgeois D (2019). Mechanistic investigation of mEos4b reveals a strategy to reduce track interruptions in sptPALM. Nat Methods 16, 707–710.
Ehrlich M, Boll W, Van Oijen A, Hariharan R, Chandran K, Nibert ML, Kirchhausen T (2004). Endocytosis by random initiation and stabilization of clathrin-coated pits. Cell 118, 591–605.
Grabski A, Mehler M, Drott D (2005). The Overnight Express Autoinduction System: high-density cell growth and protein expression while you sleep. Nat Methods 2, 233–235.
Gustafsson MG (2000). Surpassing the lateral resolution limit by a factor of two using structured illumination microscopy. J Microsc 198, 82–87.
Habuchi S, Ando R, Dedecker P, Verheijen W, Mizuno H, Miyawaki A, Hofkens J (2005). Reversible single-molecule photoswitching in the GFP-like fluorescent protein Dronpa. Proc Natl Acad Sci USA 102, 9511–9516.
Heilemann M, Margeat E, Kasper R, Sauer M, Tinnefeld P (2005). Carbocyanine dyes as efficient reversible single-molecule optical switch. J Am Chem Soc 127, 3801–3806.
Hell SW, Wichmann J (1994). Breaking the diffraction resolution limit by stimulated emission: stimulated-emission-depletion fluorescence microscopy. Opt Lett 19, 780–782.
Hutchison CDM, Cordon-Preciado V, Morgan RML, Nakane T, Ferreira J, Dorlhiac G, Sanchez-Gonzalez A, Johnson AS, Fitzpatrick A, Fare C, *et al*. (2017). X-ray free electron laser determination of crystal structures of dark and light states of a reversibly photoswitching fluorescent protein at room temperature. Int J Mol Sci 18, 1918.
Johnson E, Kaufmann R (2017). Preserving the photoswitching ability of standard fluorescent proteins for correlative in-resin super-resolution and electron microscopy. Methods Cell Biol 140, 49–67.
Joosen L, Hink MA, Gadella TW, Goedhart J (2014). Effect of fixation procedures on the fluorescence lifetimes of *Aequoreavictoria* derived fluorescent proteins. J Microsc 256, 166–176.
Khan AO, Simms VA, Pike JA, Thomas SG, Morgan NV (2017). CRISPR-Cas9 mediated labelling allows for single molecule imaging and resolution. Sci Rep 7, 8450.
Klar TA, Jakobs S, Dyba M, Egner A, Hell SW (2000). Fluorescence microscopy with diffraction resolution barrier broken by stimulated emission. Proc Natl Acad Sci USA 97, 8206–8210.
Leterrier C, Potier J, Caillol G, Debarnot C, Rueda Boroni F, Dargent B (2015). Nanoscale architecture of the axon initial segment reveals an organized and robust scaffold. Cell Rep 13, 2781–2793.
Levet F, Hosy E, Kechkar A, Butler C, Beghin A, Choquet D, Sibarita JB (2015). SR-Tesseler: a method to segment and quantify localization-based super-resolution microscopy data. Nat Methods 12, 1065–1071.
Leyton-Puig D, Isogai T, Argenzio E, van den Broek B, Klarenbeek J, Janssen H, Jalink K, Innocenti M (2017). Flat clathrin lattices are dynamic actin-controlled hubs for clathrin-mediated endocytosis and signalling of specific receptors. Nat Commun 8, 16068.
Lippincott-Schwartz J, Patterson GH (2009). Photoactivatable fluorescent proteins for diffraction-limited and super-resolution imaging. Trends Cell Biol 19, 555–565.
Lu-Walther HW, Hou W, Kielhorn M, Arai Y, Nagai T, Kessels MM, Qualmann B, Heintzmann R (2016). Nonlinear structured illumination using a fluorescent protein activating at the readout wavelength. PLoS One 11, e0165148.
McKinney SA, Murphy CS, Hazelwood KL, Davidson MW, Looger LL (2009). A bright and photostable photoconvertible fluorescent protein. Nat Methods 6, 131.
Olivier N, Keller D, Gonczy P, Manley S (2013). Resolution doubling in 3D-STORM imaging through improved buffers. PLoS One 8, e69004.
Ovesný M, K ížek P, Borkovec J, Svindrych Z, Hagen GM (2014). ThunderSTORM: a comprehensive ImageJ plug-in for PALM and STORM data analysis and super-resolution imaging. Bioinformatics 30, 2389–2390.
Paez-Segala MG, Sun MG, Shtengel G, Viswanathan S, Baird MA, Macklin JJ, Patel R, Allen JR, Howe ES, Piszczek G, *et al*. (2015). Fixation-resistant photoactivatable fluorescent proteins for CLEM. Nat Methods 12, 215–218.
Pennacchietti F, Serebrovskaya EO, Faro AR, Shemyakina II, Bozhanova NG, Kotlobay AA, Gurskaya NG, Bodén A, Dreier J, Chudakov DM, *et al*. (2018). Fast reversibly photoswitching red fluorescent proteins for live-cell RESOLFT nanoscopy. Nat Methods 15, 601–604.
Rust MJ, Bates M, Zhuang X (2006). Sub-diffraction-limit imaging by stochastic optical reconstruction microscopy (STORM). Nat Methods 3, 793–795.
Sarkisyan KS, Goryashchenko AS, Lidsky PV, Gorbachev DA, Bozhanova NG, Gorokhovatsky AY, Pereverzeva AR, Ryumina AP, Zherdeva VV, Savitsky AP, *et al*. (2015). Green fluorescent protein with anionic tryptophan-based chromophore and long fluorescence lifetime. Biophys J 109, 380–389.
Shaner NC, Lambert GG, Chammas A, Ni Y, Cranfill PJ, Baird MA, Sell BR, Allen JR, Day RN, Israelsson M, *et al*. (2013). A bright monomeric green fluorescent protein derived from *Branchiostomalanceolatum*. Nat Methods 10, 407–409.
Shcherbakova DM, Sengupta P, Lippincott-Schwartz J, Verkhusha VV (2014). Photocontrollable fluorescent proteins for super-resolution imaging. Annu Rev Biophys 43, 303–329.
Shinoda H, Lu K, Nakashima R, Wazawa T, Noguchi K, Matsuda T, Nagai T (2019). Acid-tolerant reversibly switchable green fluorescent protein for super-resolution imaging under acidic conditions. Cell Chem Biol 26, 1469–1479.e1466.
Shinoda H, Ma Y, Nakashima R, Sakurai K, Matsuda T, Nagai T (2018). Acid-tolerant monomeric GFP from *Olindiasformosa*. Cell Chem Biol 25, 330–338.e337.
Staszowska AD, Fox-Roberts P, Hirvonen LM, Peddie CJ, Collinson LM, Jones GE, Cox S (2018). The Rényi divergence enables accurate and precise cluster analysis for localization microscopy. Bioinformatics 34, 4102–4111.
Studier FW (2005). Protein production by auto-induction in high density shaking cultures. Protein Expr Purif 41, 207–234.
Tachikawa M, Morone N, Senju Y, Sugiura T, Hanawa-Suetsugu K, Mochizuki A, Suetsugu S (2017). Measurement of caveolin-1 densities in the cell membrane for quantification of caveolar deformation after exposure to hypotonic membrane tension. Sci Rep 7, 7794.
van de Linde S, Krsti I, Prisner T, Doose S, Heilemann M, Sauer M (2011). Photoinduced formation of reversible dye radicals and their impact on super-resolution imaging. Photochem Photobiol Sci 10, 499–506.
Virant D, Traenkle B, Maier J, Kaiser PD, Bodenhöfer M, Schmees C, Vojnovic I, Pisak-Lukáts B, Endesfelder U, Rothbauer U (2018). A peptide tag-specific nanobody enables high-quality labeling for dSTORM imaging. Nat Commun 9, 930.
Wiedenmann J, Ivanchenko S, Oswald F, Schmitt F, Röcker C, Salih A, Spindler KD, Nienhaus GU (2004). EosFP, a fluorescent marker protein with UV-inducible green-to-red fluorescence conversion. Proc Natl Acad Sci USA 101, 15905–15910.
Zhang M, Chang H, Zhang Y, Yu J, Wu L, Ji W, Chen J, Liu B, Lu J, Liu Y, *et al*. (2012). Rational design of true monomeric and bright photoactivatable fluorescent proteins. Nat Methods 9, 727–729.
Zhang X, Chen X, Zeng Z, Zhang M, Sun Y, Xi P, Peng J, Xu P (2015). Development of a reversibly switchable fluorescent protein for super-resolution optical fluctuation imaging (SOFI). ACS Nano 9, 2659–2667.
Zhang X, Zhang M, Li D, He W, Peng J, Betzig E, Xu P (2016). Highly photostable, reversibly photoswitchable fluorescent protein with high contrast ratio for live-cell super-resolution microscopy. Proc Natl Acad Sci USA 113, 10364–10369.